PHY Security Enhancement Exploiting STAR-RIS for Dual-functional Radar-Communication

Chao Wang[1,2], Cheng-Cai Wang[3], Zan Li[1], Derrick Wing Kwan Ng[4], and Kai-Kit Wong[5]
[1]State Key Laboratory of Integrated Service Network, Xidian University, Xi'an 710071, China
[2]Key Laboratory of Broadband Wireless Communication and Sensor Network Technology, NJUPT, Nanjing 210003, China
[3]School of Automation Science and Electrical Engineering, Beihang University, Beijing 100191, China
[4]School of Electrical Engineering and Telecommunications, University of New South Wales, Sydney, 2052, Australia
[5]Department of Electronic and Electrical Engineering, University College London, London, WC1E 6BT, UK
Email: drchaowang@126.com, ccwang@pku.edu.cn, zanli@xidian.edu.cn, w.k.ng@unsw.edu.au, kai-kit.wong@ucl.ac.uk

***Abstract*—Considering a simultaneously transmitting and reflecting reconfigurable intelligent surfaces (STAR-RIS)-aided dual-functional radar-communications (DFRC) system, this paper proposes a symbol-level precoding-based scheme for enhancing the physical layer (PHY) security of the confidential information transmission and performing target sensing simultaneously. Specifically, the STAR-RIS-aided DFRC system design objective is to maximize the average received radar sensing power subject to the quality-of-service constraints for multiple communication users, the security constraint for multiple potential eavesdroppers, as well as various practical waveform design restrictions. However, the formulated problem is challenging to handle due to its nonconvexity. To address these issues, we propose a distance-majorization induced low-complexity algorithm to obtain an efficient solution. Simulation results confirm the effectiveness of the STAR-RIS in improving the DFRC performance.**

***Index Terms*—STAR-RIS, dual-functional radar-communication, symbol-level precoding, distance-majorization.**

I. Introduction

The upcoming sixth-generation (6G) networks will enable a plethora of emerging applications such as autonomous driving and smart factories, etc. Hence, there is an urgent need to integrate radar sensing capability into the next-generation wireless networks to establish perceptive mobile networks via the notion of dual-functional radar-communications (DFRC) [1]. One of the promising approaches for realizing DFRC is to adopt communication waveforms to perform radar sensing, where the object information can be extracted from the received echo signals [2], [3]. Besides, the recently proposed STAR-RIS has enabled the signal transmission and reflection simultaneously, which achieves a larger coverage area than the reconfigurable intelligent surfaces (RIS) technique [4]–[7]. Recently, some works such as [8], have studied the STAR-RIS-aided DFRC. However, the relevant research is still in infancy.

Moreover, compared with radar systems, communication-centric DFRC systems encounter serious security problems, since communication signal-enabled radar sensing are generally susceptible to potential eavesdropping attacks due to the reuse of information-carrying signal waveform [9]–[11]. Compared with DFRC, the security threat in STAR-RIS aided DFRC is severer due to the extra strong path introduced by STAR-RIS to the malicious radar targets. To the best of our knowledge, the physical layer (PHY) security scheme for STAR-RIS-aided DFRC has not been considered before.

Against this background, this work investigates the PHY security (PLS) of STAR-RIS-aided DFRC. Considering that the multiple malicious targets may potentially eavesdrop the confidential information intended to the secure user, we adopt the symbol-level precoding technique to design an efficient deception strategy for securing DFRC. In particular, we investigate the joint optimization of the signal waveform, the active beamforming at the base station (BS), the passive transmit and reflective beamforming at the RIS for maximizing the radar sensing power of DFRC while guaranteeing the communication reliability and security. Although the formulated joint optimization problem is nonconvex, we propose a low-complexity distance-majorization-based iterative algorithm.

Notation: χ_k^2 denotes a central chi-squared random variable with k DoF. $\mathcal{R}\left(a\right)$ and $\mathcal{I}\left(a\right)$ denotes the real and imaginary part of a complex number a. $\left(\cdot\right)^T$, $\left(\cdot\right)^H$, and $||\cdot||_2$ denote the transpose, the conjugate transpose, and the L_2 norm, respectively; $\mathrm{Tr}\left(\cdot\right)$ and $\left(\cdot\right)^{-1}$ denote the trace and inverse of an input matrix, respectively; $\ln(\cdot)$ denotes the natural logarithm; $\mathbf{a}./\mathbf{b}$ denotes the element-wise division of the two vectors; $\mathbf{x}\sim\mathcal{CN}\left(\mathbf{\Lambda},\mathbf{\Delta}\right)$ denotes the complex Gaussian vector $\mathbf{x}$ with mean vector $\mathbf{\Lambda}$ and covariance matrix $\mathbf{\Delta}$. $\mathbf{I}_N$ is the $N\times N$ identity matrix. $\mathrm{vec}(\cdot)$ is the vectorization operator. $\otimes$ denotes the Kronecker product. $\mathbf{V}\succeq\mathbf{0}$ is a Hermitian positive semi-definite matrix. $x\sim\exp(\lambda)$ denotes an exponential random variable with mean λ. $\mathrm{diag}(\cdot)$ denotes a diagonal matrix. $\mathcal{O}(\cdot)$ is the big-O notation.

Corresponding authors: Chao Wang; Cheng-Cai Wang.

The work of C. C. Wang is supported by Beijing Nova Program. The work of C. Wang is supported by the National Natural Science Foundation of China under Grants 61801518, the Key Research and Development Program of Shaanxi (ProgramNo. 2022KW-03), the Defense Industrial Technology Development Program under Grant JCKY2021608B001, the Fundamental Research Funds for the Central Universities under Grant ZYTS23177, the open research fund of Key Lab of Broadband Wireless Communication and Sensor Network Technology (NJUPT). The work of K. K. Wong is supported by the Engineering and Physical Sciences Research Council (EPSRC) under grant EP/V052942/1. The work of D. W. K. Ng is supported by the Australian Research Council's Discovery Project (DP210102169).

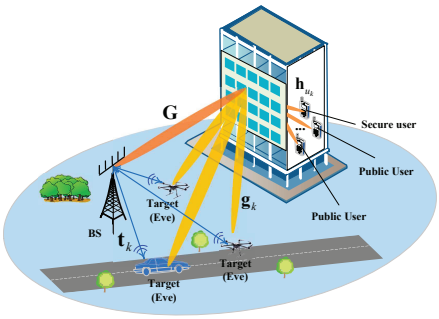

Fig. 1. An illustration of the considered STARS-aided DFRC system.

II. System Model and Performance Metric

A. System Model

We consider a STAR-RIS-enabled DFRC system as illustrated in Fig. 1, where a multi-antenna dual-functional BS serves K_u downlink single-antenna users while detecting K_e point-like targets with the help of a STAR-RIS. The BS is equipped with N_t transmitting antennas where $N_t \geq K_u$. Besides, the information intended to the secure user is confidential while the information transmitted to the remaining users is public. Similar to [12], we assume that the STAR-RIS is equipped with a uniform linear array (ULA) consisting of a total of N T-R elements. Also, the direct channel from the BS to the users are blocked. Multiple targets are assumed to be malicious single-antenna eavesdroppers (Eves) which wiretaps the confidential information intended to the secure user.

In this work, we propose to adopt the symbol-level precoding technique to perform signal broadcasting and radar sensing simultaneously. In particular, the transmitted signals in the lth time slot are the non-linear mapping from the information symbols intended for the K_u users, $\mathbf{x}[l] \triangleq [x_1[l], \ldots, x_{K_u}[l]]^T$ to the baseband signal transmitted from the N_t antennas, $\mathbf{s}[l] \triangleq [s_1[l], \ldots, s_{N_t}[l]]^T$. This work concentrates on studying the joint optimization of the transmission signal $\mathbf{s}[l]$, the matrices of the transmission coefficients and reflection coefficients at the STAR-IRS, i.e., $\mathbf{\Theta}_t \triangleq \text{diag}\left(\tau_{t,1}e^{j\theta_{t,1}}, \ldots, \tau_{t,N}e^{j\theta_{t,N}}\right)$ and $\mathbf{\Theta}_r \triangleq \text{diag}\left(\tau_{r,1}e^{j\theta_{r,1}}, \ldots, \tau_{r,N}e^{j\theta_{r,N}}\right)$, respectively, where $\tau_{t,i}$ and $0 \leq \theta_{t,i} \leq 2\pi$ are the amplitude and phase of the ith transmission coefficient, respectively. Besides, $\tau_{r,i}$ and $\theta_{r,i}$ are the amplitude and phase of the ith reflection coefficient, respectively. Following the existing works on DFRC [13], the joint design is formulated as an optimization problem that maximizes the total illumination power along the target directions taking into account the constructive interference (CI)-type constraints on the communication users, security constraints on the secure user, and other practical constraints on the transmit beampatterns including the peak-to-average-power ratio and similarity constraints.

B. Multiuser Communications Performance Metric

Following [2], the data symbols are assumed to be modulated using the phase-shift-keying (PSK) scheme. At the lth time slot, the symbol-level precoded signal vector is $\mathbf{s}[l]$ and the received signal at the kth user is given by

$$y_{u_k}[l] = \mathbf{h}_{u_k}^H \mathbf{\Theta}_t \mathbf{G}\mathbf{S}(:,l) + n_{u_k}[l],\ l \in \mathcal{L}, \tag{1}$$

where $\mathcal{L} \triangleq [1, \ldots, L]$, $\mathbf{S} \triangleq [\mathbf{s}[1], \ldots, \mathbf{s}[L]]$ is the transmit signal matrix from the BS over the L time slots, $\mathbf{S}(:,l)$ denotes the lth column of $\mathbf{S}$, and $n_{u_k}[l] \sim \mathcal{CN}(0, \sigma^2)$ is the noise received at the kth user. Besides, the channels are modeled as $\mathbf{G} \triangleq \sqrt{l_{br}}\bar{\mathbf{G}} \in \mathbb{C}^{N \times N_t}$ and $\mathbf{h}_{u_k}^H \triangleq \sqrt{l_{ru_k}}\bar{\mathbf{h}}_{u_k}^H \in \mathbb{C}^{1 \times N}$, where l_{xy} is the large-scale path loss of the link x-to-y and $xy \in \{br, ru_k\}$ denotes the direction of the link from x to y. The small-scale fading coefficients $\bar{\mathbf{G}} \in \mathbb{C}^{N \times N_t}$ and $\bar{\mathbf{h}}_{u_k}^H \in \mathbb{C}^{1 \times N_t}$ are modeled as Rician fading channels [5], [14], i.e.,

$$\bar{\mathbf{G}} = \sqrt{\frac{\kappa_{\text{G}}}{1+\kappa_{\text{G}}}}\bar{\mathbf{G}}_{\text{LOS}} + \sqrt{\frac{1}{1+\kappa_G}}\bar{\mathbf{G}}_{\text{NLOS}}, \tag{2}$$

$$\bar{\mathbf{h}}_{u_k}^H = \sqrt{\frac{\kappa_{u_k}}{1+\kappa_{u_k}}}\bar{\mathbf{h}}_{u_k,\text{LOS}} + \sqrt{\frac{1}{1+\kappa_{u_k}}}\bar{\mathbf{h}}_{u_k,\text{NLOS}}^H, \tag{3}$$

respectively, where $\kappa_{\text{G}} \geq 0$ and $\kappa_{u_k} \geq 0$ are the corresponding Rician factors. $\bar{\mathbf{G}}_{\text{NLOS}}$ and $\bar{\mathbf{h}}_{u_k,\text{NLOS}}^H$ are the non-line-of-sight (NLOS) components which are modeled as Rayleigh fading channels. Denoting ω_B and ω_R as the effective angle-of-departure (AOD) and angle-of-arrival (AOA) of the link BS-to-STAR-RIS, respectively, the line-of-sight (LOS) channel from the BS to the STAR-RIS is $\bar{\mathbf{G}}_{\text{LOS}} \triangleq \mathbf{a}_N^T(\omega_R)\,\mathbf{a}_{N_t}(\omega_B)$, where the steering vectors are respectively given by $\mathbf{a}_N(\omega_R) = \frac{1}{\sqrt{N}}\left[1, e^{-j2\pi\frac{\sin(\omega_R)}{2}}, \ldots, e^{-j2\pi\frac{(N-1)\sin(\omega_R)}{2}}\right]^T$, $\mathbf{a}_{N_t}(\omega_B) = \frac{1}{\sqrt{N_t}}\left[1, e^{-j2\pi\frac{\sin(\omega_B)}{2}}, \ldots, e^{-j2\pi\frac{(N_t-1)\sin(\omega_B)}{2}}\right]^T$. Accordingly, the LOS channel from the STAR-RIS to the kth user is modeled as $\bar{\mathbf{h}}_{u_k,\text{LOS}} \triangleq \mathbf{a}_N(\omega_{u_k})$, where $\mathbf{a}_N(\omega_{u_k})$ is the steering vector with the effective AOD, ω_{u_k}.

The condition for advocating the CI region is given by [15]

$$\mathcal{R}\left(\tilde{\mathbf{h}}_{l,k}^H(\mathbf{\Theta}_t)\,\mathbf{s}\right) \geq \gamma_{u_k},\ \mathcal{I}\left(\hat{\mathbf{h}}_{l,k}^H(\mathbf{\Theta}_t)\,\mathbf{s}\right) \geq \gamma_{u_k}, \tag{4}$$

where $\gamma_{u_k} \triangleq \sigma\sqrt{\Gamma_{u_i}}\sin\Phi$. $\tilde{\mathbf{h}}_{l,k}^H(\mathbf{\Theta}_t)$ and $\hat{\mathbf{h}}_{l,k}^H(\mathbf{\Theta}_t)$ are

$$\tilde{\mathbf{h}}_{l,k}^H(\mathbf{\Theta}_t) \triangleq \mathbf{e}_{l,L}^T \otimes \left(\mathbf{h}_{u_k}^H \mathbf{\Theta}_t \mathbf{G}\right) e^{-j\angle x_k(l)}\left(\sin(\Phi) + e^{-j\frac{\pi}{2}}\cos(\Phi)\right),$$

$$\hat{\mathbf{h}}_{l,k}^H(\mathbf{\Theta}_t) \triangleq \mathbf{e}_{l,L}^T \otimes \left(\mathbf{h}_{u_k}^H \mathbf{\Theta}_t \mathbf{G}\right) e^{-j\angle x_k(l)}\left(\sin(\Phi) - e^{-j\frac{\pi}{2}}\cos(\Phi)\right),$$

where $\angle x_k(l)$ is the angle of symbol $x_k(l)$.

C. Radar Sensing Performance Metric

The signals from the BS and the STAR-RIS are superimposed at the kth radar targets in the lth time slot, given by

$$y_{r_k}(l) = \left(\sqrt{l_{bu_k}}\mathbf{a}_{N_t}^T(\psi_k) + \sqrt{l_{ru_k}}\mathbf{a}_N^T(\theta_k)\mathbf{\Theta}_r\mathbf{G}\right)\mathbf{S}(:,l),$$

where l_{bu_k} is the path loss from the BS to the kth target and l_{ru_k} is the path loss from STAR-RIS to the kth target. Besides, $\mathcal{K}_e \triangleq \{1 \ldots, K_e\}$, ψ_k and θ_k are the effective AOD from the BS and the RIS to the kth radar target. Furthermore, $\mathbf{a}_{N_t}(\psi_k)$ is the steering vector from the BS to the kth target and $\mathbf{a}_N(\theta_k)$ is the steering vector from the STAR-RIS to the kth target [16].

Accordingly, the average beampattern over the L time slots at the kth target direction can be derived as

$$P(\theta_k,\psi_k)=\mathbf{b}\left(\psi_k,\theta_k\right)\mathbf{S}\mathbf{S}^H\mathbf{b}^H\left(\psi_k,\theta_k\right)/L,\ k\in\mathcal{K}_e, \quad (5)$$

where $\mathbf{b}\left(\psi_k,\theta_k\right)=\sqrt{l_{bu_k}}\mathbf{a}_{N_t}^T(\psi_k)+\sqrt{l_{ru_k}}\mathbf{a}_N^T(\theta_k)\mathbf{\Theta}_r\mathbf{G}$, and the angles ψ_k and θ_k are determined by the relative locations of the kth target, IRS, and the BS. Besides, having a low peak-to-average-power ratio (PAPR) is an important characteristic of modern radar systems and the corresponding constraint is

$$\max_{1\le l\le L}|\mathbf{s}(l)|^2/\left(\frac{1}{N_tL}\mathbf{s}^H\mathbf{s}\right)\le\eta. \quad (6)$$

D. Secure Communication Performance Metric

We propose a deceiving-based secure transmission scheme, where the unclassified signal is designed to lie in the constructive region of multiple radar targets. Then, malicious targets mistake the unclassified signal for confidential signals. To guarantee an effective deception, the minimum Euclidean distance from the noise-free wiretapped signal to the decision boundary of any public signals is adopted as the quality-of-service (QoS), given by

$$\mathcal{R}\left(\tilde{\mathbf{g}}_{l,k}^H\left(\mathbf{\Theta}_r\right)\mathbf{s}\right)\ge\eta_{e_k},\ \mathcal{I}\left(\hat{\mathbf{g}}_{l,k}^H\left(\mathbf{\Theta}_r\right)\mathbf{s}\right)\ge\eta_{e_k},\forall k\in\mathcal{K}_e, \quad (7)$$

where $\eta_{e_k}\triangleq\sigma\sqrt{\Gamma_{e_k}}\sin(\Phi)$, $\tilde{\mathbf{g}}_{l,k}^H$ and $\hat{\mathbf{g}}_{l,k}^H$ are given by $\tilde{\mathbf{g}}_{l,k}^H\left(\mathbf{\Theta}_r\right)\triangleq\mathbf{e}_{l,L}^T\otimes\left(\mathbf{t}_{e_k}^H+\mathbf{g}_{e_k}^H\mathbf{\Theta}_r\mathbf{G}\right)\times e^{-j\angle x_{\hat{u}}(l)}\left(\sin(\Phi)+e^{-j\frac{\pi}{2}}\cos(\Phi)\right)$, $\hat{\mathbf{g}}_{l,k}^H\left(\mathbf{\Theta}_r\right)\triangleq\mathbf{e}_{l,L}^T\otimes\left(\mathbf{t}_{e_k}^H+\mathbf{g}_{e_k}^H\mathbf{\Theta}_r\mathbf{G}\right)e^{-j\angle x_{\hat{u}}(l)}\times\left(\sin(\Phi)-e^{-j\frac{\pi}{2}}\cos(\Phi)\right)$, respectively, where $x_{\hat{u}}(l)$ denotes the symbol intended to any public user in the lth slot. Besides, we have

$$\mathbf{g}_{l,k}^H=\sqrt{\frac{\kappa_{\mathbf{g}_{l,k}}}{1+\kappa_{\mathbf{g}_{l,k}}}}\mathbf{a}_N^T(\theta_k)+\sqrt{\frac{1}{1+\kappa_{\mathbf{g}_{l,k}}}}\mathbf{g}_{l,k,\mathrm{NLOS}}^H, \quad (8)$$

$$\mathbf{t}_{l,k}^H=\sqrt{\frac{\kappa_{\mathbf{t}_{l,k}}}{1+\kappa_{\mathbf{t}_{l,k}}}}\mathbf{a}_{N_t}^T(\psi_k)+\sqrt{\frac{1}{1+\kappa_{\mathbf{t}_{l,k}}}}\mathbf{t}_{l,k,\mathrm{NLOS}}^H. \quad (9)$$

The components in (8) and (9) are defined similarly as their counterparts in (2) and (3), respectively. Constraint (7) restricts the wiretapped signal received at the multiple radar targets to fall into the decision region that favours any public signals to deceive the malicious targets.

E. Joint Optimization Problem Formulation

The joint design of the signal waveform and beamforming $(\mathbf{\Theta}_t,\mathbf{\Theta}_r)$ can be formulated as

$$\underset{\mathbf{s},\mathbf{\Theta}_t,\mathbf{\Theta}_r}{\text{maximize}}\ \sum_{i=1}^{K_e}P(\theta_i,\psi_i) \quad (10a)$$

$$\text{s.t. }||\mathbf{s}-\mathbf{s}_0||_2\le\sqrt{\epsilon L}, \quad (10b)$$

$$\mathbf{s}^H\mathbf{s}=LP_t, \quad (10c)$$

$$\mathbf{s}^H\mathbf{E}_m\mathbf{s}\le\frac{P_t\eta}{N_t},\ 1\le m\le N, \quad (10d)$$

$$(4),\ (7),\ k\in\mathcal{K}_u,\ k\in\mathcal{K}_e,\ l\in\mathcal{L}, \quad (10e)$$

$$[\mathbf{\Theta}_r]_{m,m}^2+[\mathbf{\Theta}_t]_{m,m}^2=1,\ 1\le m\le N, \quad (10f)$$

where $\mathbf{s}=\mathrm{vec}\left(\mathbf{S}\right)$, ϵ is a customized parameter for controlling the similarity level, and constraint (10b) is the l_2 norm similarity constraint for shaping the transmission signal waveform to mimic the reference signal $\mathbf{s}_0$, e.g., pulse compression. Constraints (10c) and (10d) denote the PAPR constraint (6). Besides, $\mathbf{E}_m$ is an $N_tL\times N_tL$ diagonal matrix whose (m,m) element is either 1 or 0. Constraint (10f) denotes the amplitude constraints on the transmission and reflection elements [6]. It is clear that problem (10) is nonconvex and obtaining its globally optimal solution is very challenging.

III. Distance-Majorization Induced Low-Complexity Algorithm

To handle the coupling among optimization variables, we adopt the alternating optimization (AO) to optimize $\mathbf{s}$ and $(\mathbf{\Theta}_t,\mathbf{\Theta}_r)$ in an alternating iteration.

A. Distance-Majorization Algorithm for Optimizing the Signal Waveform

With fixed $\mathbf{\Theta}_t$ and $\mathbf{\Theta}_r$, the optimization of the waveform $\mathbf{s}$ can be formulated as follows

$$\underset{\mathbf{s}}{\text{maximize}}\ \mathbf{s}^H\mathbf{B}\mathbf{s} \quad (11a)$$

$$\text{s.t. }||\mathbf{s}||_2^2=LP_t,\ ||s_i(l)||_2^2\le\frac{P_t\eta}{N_t},\ 1\le i\le N_t,\ 1\le l\le L, \quad (11b)$$

$$\mathcal{R}\left(-\tilde{\mathbf{h}}_{l,k}^H\left(\mathbf{\Theta}_t\right)\mathbf{s}\right)\le-\gamma_{u_k},\ \mathcal{R}\left(-\hat{\mathbf{h}}_{l,k}^H\left(\mathbf{\Theta}_t\right)\mathbf{s}\right)\le-\gamma_{u_k},\ k\in\mathcal{K}_u,\ l\in\mathcal{L}, \quad (11c)$$

$$\mathcal{R}\left(-\tilde{\mathbf{g}}_{l,k}^H\left(\mathbf{\Theta}_r\right)\mathbf{s}\right)\le-\eta_{e_k},\ \mathcal{R}\left(-\hat{\mathbf{g}}_{l,k}^H\left(\mathbf{\Theta}_r\right)\mathbf{s}\right)\le-\eta_{e_k},\ k\in\mathcal{K}_e,\ l\in\mathcal{L}, \quad (11d)$$

$$||\mathbf{s}-\mathbf{s}_0||_2\le\sqrt{\epsilon L}, \quad (11e)$$

where $\mathbf{A}\left(\psi_i,\theta_i\right)\triangleq\mathbf{b}^H\left(\psi_i,\theta_i\right)\mathbf{b}\left(\psi_i,\theta_i\right)$ and $\mathbf{B}=\sum_{i=1}^{K_e}\left(\mathbf{I}_L\otimes\mathbf{A}\left(\psi_i,\theta_i\right)\right)$.

To design an efficient algorithm to handle problem (11), we propose a distance-majorization induced iterative algorithm. In particular, we employ the Courant's penalty method to incorporate constraints (11b)-(11d) into the objective function, and then, a distance-majorization [17] induced low-complexity algorithm is proposed to the problem with the modified objective function. To facilitate the algorithm design, we first convert the complex-valued formulation of problem (11) into its real-valued counterpart given by

$$\underset{\mathbf{s}}{\text{maximize}}\ \hat{\mathbf{s}}^T\hat{\mathbf{B}}\hat{\mathbf{s}}$$

$$\text{s.t. }||\hat{\mathbf{s}}||_2^2=LP_t,\ ||\left[\hat{\mathbf{s}}(n),\hat{\mathbf{s}}(LN_t+n)\right]||_2^2\le\frac{P_t\eta}{N_t}, \quad (12a)$$

$$\tilde{\mathbf{f}}_{l,k}^T\left(\mathbf{\Theta}_t\right)\hat{\mathbf{s}}\le-\gamma_{u_k},\ \hat{\mathbf{f}}_{l,k}^T\left(\mathbf{\Theta}_t\right)\hat{\mathbf{s}}\le-\gamma_{u_k},k\in\mathcal{K}_u,\ l\in\mathcal{L}, \quad (12b)$$

$$\tilde{\mathbf{t}}_{l,k}^T\left(\mathbf{\Theta}_r\right)\hat{\mathbf{s}}\le-\eta_{e_k},\ \hat{\mathbf{t}}_{l,k}^T\left(\mathbf{\Theta}_r\right)\hat{\mathbf{s}}\le-\eta_{e_k},k\in\mathcal{K}_e,\ l\in\mathcal{L}, \quad (12c)$$

$$||\hat{\mathbf{s}}-\hat{\mathbf{s}}_0||_2\le\sqrt{\epsilon L}, \quad (12d)$$

where $\hat{\mathbf{s}} = [\mathcal{R}(\mathbf{s}), \mathcal{I}(\mathbf{s})]^T$, $\hat{\mathbf{s}}_0 = [\mathcal{R}(\mathbf{s}_0), \mathcal{I}(\mathbf{s}_0)]^T$, $\hat{\mathbf{B}} = \begin{bmatrix} \mathcal{R}(\mathbf{B}), & -\mathcal{I}(\mathbf{B}) \\ \mathcal{I}(\mathbf{B}), & \mathcal{R}(\mathbf{B}) \end{bmatrix}$, $\hat{\mathbf{f}}_{l,k}^T(\mathbf{\Theta}_t) = -\left[\mathcal{R}\left(\hat{\mathbf{h}}_{l,k}^T\right), -\mathcal{I}\left(\hat{\mathbf{h}}_{l,k}^T\right)\right]$, $\tilde{\mathbf{t}}_{l,k}^T(\mathbf{\Theta}_t) = -\left[\mathcal{R}\left(\tilde{\mathbf{g}}_{l,k}^T\right), -\mathcal{I}\left(\tilde{\mathbf{g}}_{l,k}^T\right)\right]$, $\hat{\mathbf{t}}_{l,k}^T(\mathbf{\Theta}_t) = -\left[\mathcal{R}\left(\hat{\mathbf{g}}_{l,k}^T\right), -\mathcal{I}\left(\hat{\mathbf{g}}_{l,k}^T\right)\right]$.

Then, with the Courant's penalty method, a penalized optimization problem is built as

$$\underset{\hat{\mathbf{s}},\tilde{y}_k^u,\hat{y}_k^u,\tilde{y}_k^e,\hat{y}_k^e}{\text{maximize}} \ \hat{\mathbf{s}}^T\hat{\mathbf{B}}\hat{\mathbf{s}} - \frac{\rho}{2}\Delta(\hat{\mathbf{s}}) \tag{13a}$$

$$\text{s.t. } \tilde{y}_{l,k}^u = \tilde{\mathbf{f}}_{l,k}^H(\mathbf{\Theta}_t)\hat{\mathbf{s}},\ \hat{y}_{l,k}^u = \hat{\mathbf{f}}_{l,k}^H(\mathbf{\Theta}_t)\hat{\mathbf{s}},\ k \in \mathcal{K}_u,\ l \in \mathcal{L},$$
$$\tilde{y}_{l,k}^e = \tilde{\mathbf{t}}_{l,k}^H(\mathbf{\Theta}_r)\hat{\mathbf{s}},\ \hat{y}_{l,k}^e = \hat{\mathbf{t}}_{l,k}^H(\mathbf{\Theta}_r)\hat{\mathbf{s}},\ k \in \mathcal{K}_e,\ l \in \mathcal{L},$$
$$||\hat{\mathbf{s}} - \hat{\mathbf{s}}_0||_2 \le \sqrt{\epsilon L}, \tag{13b}$$

where $\rho > 0$ is the penalty parameter and $\Delta(\hat{\mathbf{s}}) \triangleq \sum_{k=1}^{K_u}\sum_{l=1}^{L}\left(\text{dist}^2\left(\tilde{y}_{l,k}^u, \Xi\right) + \text{dist}^2\left(\hat{y}_{l,k}^u, \Xi\right)\right) + \text{dist}^2(\hat{\mathbf{s}}, \Omega) + \sum_{k=1}^{K_e}\sum_{l=1}^{L}\left(\text{dist}^2\left(\hat{y}_{l,k}^e, \Psi\right) + \text{dist}^2\left(\tilde{y}_{l,k}^e, \Psi\right)\right)$. Besides, Ω, Ξ, and Ψ are feasible sets determined by constraints (12a), (12b), and (12c), respectively.

Theorem 1: As $\rho \to +\infty$, the solution of problem (13) converges to the optimal solution of problem (12).

Proof: The proof is omitted due to the space limitation. ■

Although constraints (12a), (12b), and (12c) have been incorporated into the objective function, calculating the minimum distance $\Delta(\hat{\mathbf{s}})$ still involves solving multiple optimization problems whose computational complexity can be exceedingly high. As an alternative, by employing majorization-minimization (MM), we approximate problem (13) as a sequence of convex optimization problems, given by

$$\underset{\hat{\mathbf{s}}}{\text{maximize}}\ F(\hat{\mathbf{s}}),\ \text{s.t. } (13b), \tag{14}$$

where $F(\hat{\mathbf{s}}) \triangleq \hat{\mathbf{s}}^T\hat{\mathbf{B}}\hat{\mathbf{s}} - \frac{\rho}{2}\sum_{k=1}^{K_u}\sum_{l=1}^{L}\left|\left|\tilde{y}_{l,k}^u - \tilde{\gamma}_{u_k}\right|\right|_2^2 - \frac{\rho}{2}\left(\sum_{k=1}^{K_u}\sum_{l=1}^{L}\left|\left|\hat{y}_{l,k}^u - \hat{\gamma}_{u_k}\right|\right|_2^2 + \sum_{k=1}^{K_e}\sum_{l=1}^{L}\left|\left|\hat{y}_{l,k}^e - \hat{\eta}_{e_k}\right|\right|_2^2\right) - \frac{\rho}{2}\sum_{k=1}^{K_e}\sum_{l=1}^{L}\left|\left|\tilde{y}_{l,k}^e - \tilde{\eta}_{e_k}\right|\right|_2^2 - \frac{\rho}{2}||\hat{\mathbf{s}} - \check{\mathbf{s}}||_2^2 - \frac{\rho}{2}||\hat{\mathbf{s}} - \bar{\mathbf{s}}||_2^2$. Besides, $\check{\mathbf{s}}$ and $\bar{\mathbf{s}}$ are the solutions obtained by projecting $\mathbf{s}$ onto the sets $\check{\Omega} \triangleq \left\{\mathbf{s} \mid ||\hat{\mathbf{s}}||_2^2 = LP_t\right\}$ and $\bar{\Omega} \triangleq \left\{\mathbf{s} \mid ||[\hat{\mathbf{s}}(n), \hat{\mathbf{s}}(LN_t + n)]||_2^2 \le \frac{P_t\eta}{N_t}\right\}$, respectively. Moreover, $\hat{\gamma}_{u_k}$, $\tilde{\gamma}_{u_k}$, $\hat{\eta}_{e_k}$, and $\tilde{\eta}_{e_k}$ are the ones obtained by projecting $\tilde{\mathbf{f}}_{l,k}^H(\mathbf{\Theta}_t)\hat{\mathbf{s}}$, $\hat{\mathbf{f}}_{l,k}^H(\mathbf{\Theta}_t)\hat{\mathbf{s}}$, $\tilde{\mathbf{t}}_{l,k}^H(\mathbf{\Theta}_t)\hat{\mathbf{s}}$, and $\hat{\mathbf{t}}_{l,k}^H(\mathbf{\Theta}_t)\hat{\mathbf{s}}$ onto the feasible sets defined by (12b) and (12c), respectively. Although problem (14) is still nonconvex, its optimal solution still satisfies the KKT condition [18, Section 5.2]. From the KKT condition, we can obtain the optimal solution, given by

$$\hat{\mathbf{s}} = \left((2\rho + 2\lambda)\mathbf{I}_{N_tL} - 2\hat{\mathbf{B}} + \rho\mathbf{T}\right)^{-1}\mathbf{y}, \tag{15}$$

Algorithm 1 Proposed Iterative Algorithm for Problem (12)

1: Initialize $\rho = 1$, $c = 2$, $T = 30$, $\rho_{\max} \gg 1$, $\hat{\mathbf{s}}(1) = \hat{\mathbf{s}}(0) \in \mathbb{R}^{2N_tL\times 1}$, the convergence tolerance $\epsilon \ll 1$, and $m = 1$.
2: **Repeat**
3: $\hat{\mathbf{z}}(m) = \hat{\mathbf{s}}(m) + \frac{m-1}{m+2}(\hat{\mathbf{s}}(m) - \hat{\mathbf{s}}(m-1))$,
4: Project $\hat{\mathbf{z}}(m)$ on the sets defined by (12a), (12b), and (12c) and obtain $\tilde{\gamma}_{u,k}$, $\hat{\gamma}_{u,k}$, $\tilde{\eta}_{e,k}$, and $\hat{\eta}_{e,k}$, $k \in \mathcal{K}_u$, $k \in \mathcal{K}_e$, $l \in \mathcal{L}$.
5: Obtain $\hat{\mathbf{s}}$ with (15),
6: Update $\rho = \min(\rho_{\max}, c\rho)$, every T iterations
7: $m = m + 1$,
8: **Until** $||\mathbf{s}(m+1) - \mathbf{s}(m)||_2 \le \epsilon$.

where

$$\mathbf{T} = \sum_{l,k}\left(\tilde{\mathbf{f}}_{l,k}(\mathbf{\Theta}_t)\tilde{\mathbf{f}}_{l,k}^T(\mathbf{\Theta}_t) + \hat{\mathbf{f}}_{l,k}(\mathbf{\Theta}_t)\hat{\mathbf{f}}_{l,k}^T(\mathbf{\Theta}_t)\right) + \sum_{l,k}\left(\tilde{\mathbf{t}}_{l,k}(\mathbf{\Theta}_t)\tilde{\mathbf{t}}_{l,k}^T(\mathbf{\Theta}_t) + \hat{\mathbf{t}}_{l,k}(\mathbf{\Theta}_t)\hat{\mathbf{t}}_{l,k}^T(\mathbf{\Theta}_t)\right), \tag{16}$$

$$\mathbf{y} = \rho\left(\sum_{l,k}\left(\tilde{\mathbf{f}}_{l,k}(\mathbf{\Theta}_t)\tilde{r}_{u_k} + \hat{\mathbf{t}}_{l,k}(\mathbf{\Theta}_t)\hat{r}_{u_k}\right) + \check{\mathbf{s}}\right) + \rho\left(\sum_{l,k}\left(\tilde{\mathbf{t}}_{l,k}(\mathbf{\Theta}_t)\tilde{\eta}_{e_k} + \hat{\mathbf{t}}_{l,k}(\mathbf{\Theta}_t)\hat{\eta}_{e_k}\right) + \bar{\mathbf{s}}\right) + 2\lambda\mathbf{s}_0,$$

where λ can be obtained with the bisection search method for making $\lambda\left(||\hat{\mathbf{s}} - \hat{\mathbf{s}}_0||_2 - \sqrt{\epsilon L}\right) = 0$ hold.

Algorithm 1 summarizes the proposed distance-majorization induced iterative algorithm for optimizing the waveform $\hat{\mathbf{s}}$.

B. Optimization of $\mathbf{\Theta}_t$ and $\mathbf{\Theta}_r$

In this subsection, we study the joint optimization of $\mathbf{\Theta}_t$ and $\mathbf{\Theta}_r$ for the second subproblem in AO. By employing the vectorization operator given in [19, Section 1.11.2], the objective function in (10a) can be reformulated as

$$\sum_{i=1}^{M} P(\theta_i, \psi_i) = \boldsymbol{\theta}_r^H\mathbf{Q}\boldsymbol{\theta}_r + 2\mathcal{R}\left(\mathbf{q}^H\boldsymbol{\theta}_r\right) + p, \tag{17}$$

where $\mathbf{Q} \triangleq \sum_{i=1}^{M}\mathbf{L}_d^H\left(\left(\mathbf{G}\mathbf{S}\mathbf{S}^H\mathbf{G}^H\right)^T \otimes \left(\mathbf{a}_N(\theta_i)\mathbf{a}_N^H(\theta_i)\right)\right)\mathbf{L}_d$, $\mathbf{q} = \sum_{i=1}^{M}\mathbf{L}_d^H\text{vec}\left(\mathbf{a}_N(\theta_i)\mathbf{a}_{N_t}^H(\psi_i)\mathbf{S}\mathbf{S}^H\mathbf{G}^H\right)$, and $p = \sum_{i=1}^{M}\mathbf{a}_{N_t}^H(\psi_i)\mathbf{S}\mathbf{S}^H\mathbf{a}_{N_t}(\psi_i)$.

Based on the above reformulations, the joint optimization of $\mathbf{\Theta}_t$ and $\mathbf{\Theta}_r$ can be formulated as

$$\underset{\hat{\boldsymbol{\theta}}_r,\hat{\boldsymbol{\theta}}_t}{\text{maximize}}\ \hat{\boldsymbol{\theta}}_r^T\bar{\mathbf{Q}}\hat{\boldsymbol{\theta}}_r + 2\bar{\mathbf{q}}^T\hat{\boldsymbol{\theta}}_r \tag{18a}$$

$$\text{s.t.} \ \tilde{\mathbf{v}}_{l,k}\hat{\boldsymbol{\theta}}_t \le -\gamma_{u_k},\ \hat{\mathbf{v}}_{l,k}\hat{\boldsymbol{\theta}}_t \le -\gamma_{u_k},\ k \in \mathcal{K}_u,\ l \in \mathcal{L}, \tag{18b}$$
$$\tilde{\mathbf{p}}_{l,k}\hat{\boldsymbol{\theta}}_r \le -\tilde{\eta}_{e,l,k},\ \hat{\mathbf{p}}_{l,k}\hat{\boldsymbol{\theta}}_r \le -\hat{\eta}_{e,l,k},\ k \in \mathcal{K}_e,\ l \in \mathcal{L}, \tag{18c}$$
$$[\hat{\boldsymbol{\theta}}_r]_n^2 + [\hat{\boldsymbol{\theta}}_r]_{n+N}^2 + [\hat{\boldsymbol{\theta}}_t]_n^2 + [\hat{\boldsymbol{\theta}}_t]_{n+N}^2 = 1,\ 1 \le n \le N, \tag{18d}$$

where $\mathbf{v}_{l,k} \triangleq \left(\left(\mathbf{G}\mathbf{S}\mathbf{e}_{l,L}\right)^T \otimes \mathbf{h}_{u_k}^H\right)\mathbf{L}_d$, $\mathbf{p}_{l,k} \triangleq \left(\left(\mathbf{G}\mathbf{S}\mathbf{e}_{l,L}\right)^T \otimes \mathbf{g}_{e_k}^H\right)\mathbf{L}_d$, $-\tilde{\eta}_{e,l,k} = -\eta_{e_k} + \mathcal{R}\left(\tilde{\alpha}_{l,\tilde{u}}\left(\mathbf{e}_{l,L}^T \otimes \mathbf{t}_{e_k}^H\right)\mathbf{s}\right)$, $-\hat{\eta}_{e,l,k} = -\eta_{e_k} +$

$\mathcal{R}\left(\hat{\alpha}_{l,\hat{u}}\left(\mathbf{e}_{l,L}^T \otimes \mathbf{t}_{e_k}^H\right)\mathbf{s}\right)$, and

$$\bar{\mathbf{Q}} = \begin{bmatrix} \mathcal{R}(\mathbf{Q}), & -\mathcal{I}(\mathbf{Q}) \\ \mathcal{I}(\mathbf{Q}), & \mathcal{R}(\mathbf{Q}) \end{bmatrix}, \ \bar{\mathbf{q}} = [\mathcal{R}(\mathbf{q}), -\mathcal{I}(\mathbf{q})]^T, \quad (19)$$

$$\hat{\boldsymbol{\theta}}_t \triangleq [\mathcal{R}(\boldsymbol{\theta}_t), \mathcal{I}(\boldsymbol{\theta}_t)], \ \hat{\boldsymbol{\theta}}_r \triangleq [\mathcal{R}(\boldsymbol{\theta}_r), \mathcal{I}(\boldsymbol{\theta}_r)] \quad (20)$$

$$\tilde{\mathbf{v}}_{l,k} \triangleq \left[\mathcal{R}\left(-\tilde{\beta}_{l,k}\mathbf{v}_{l,k}\right), \mathcal{I}\left(\tilde{\beta}_{l,k}\mathbf{v}_{l,k}\right)\right], \quad (21)$$

$$\hat{\mathbf{v}}_{l,k} \triangleq \left[\mathcal{R}\left(-\hat{\beta}_{l,k}\mathbf{v}_{l,k}\right), \mathcal{I}\left(\hat{\beta}_{l,k}\mathbf{v}_{l,k}\right)\right], \quad (22)$$

$$\tilde{\mathbf{p}}_{l,k} \triangleq [\mathcal{R}(-\tilde{\alpha}_{l,\hat{u}}\mathbf{p}_{l,k}), \mathcal{I}(\tilde{\alpha}_{l,\hat{u}}\mathbf{p}_{l,k})], \quad (23)$$

$$\hat{\mathbf{p}}_{l,k} \triangleq [\mathcal{R}(-\hat{\alpha}_{l,\hat{u}}\mathbf{p}_{l,k}), \mathcal{I}(\hat{\alpha}_{l,\hat{u}}\mathbf{p}_{l,k})]. \quad (24)$$

Since problem (18) is nonconvex, it is challenging to solve problem (18) directly. Taking these considerations into account, we again apply the distance-majorization algorithm to handle problem (18). Firstly, an equivalent problem with an augmented objective function can be formulated as follows

$$\underset{\boldsymbol{\theta},\tilde{z}_{l,k},\hat{z}_{l,k},\tilde{x}_{l,k},\hat{x}_{l,k}}{\text{minimize}} \ -\boldsymbol{\theta}^T\mathbf{E}_r\bar{\mathbf{Q}}\mathbf{E}_r^T\boldsymbol{\theta} - 2\bar{\mathbf{q}}^T\mathbf{E}_r^T\boldsymbol{\theta} + \frac{\rho}{2}\text{dist}^2(\boldsymbol{\varpi}, \Theta) \quad (25a)$$

$$\text{s.t. } \tilde{z}_{l,k} = \tilde{\mathbf{v}}_{l,k}\mathbf{E}_t^T\boldsymbol{\theta}, \ \hat{z}_{l,k} = \hat{\mathbf{v}}_{l,k}\mathbf{E}_t^T\boldsymbol{\theta}, \quad (25b)$$

$$\tilde{x}_{l,k} = \tilde{\mathbf{p}}_{l,k}\mathbf{E}_r^T\boldsymbol{\theta}, \ \hat{x}_{l,k} = \hat{\mathbf{p}}_{l,k}\mathbf{E}_r^T\boldsymbol{\theta}, \quad (25c)$$

where $\mathbf{E}_t = [\mathbf{I}_{2N}; \mathbf{0}_{2N}]$, $\mathbf{E}_r = [\mathbf{0}_{2N}; \mathbf{I}_{2N}]$, $\boldsymbol{\varpi} \triangleq \{\boldsymbol{\theta}, \tilde{z}_{l,k}, \hat{z}_{l,k}, \tilde{x}_{l,k}, \hat{x}_{l,k}\}$, and Θ is the feasible set spanned by (18b)-(18d).

Similar to handling problem (13), we propose an MM-based iterative algorithm to handle problem (25) and a surrogate function of the objective function (25a) can be written as

$$\begin{aligned} G(\boldsymbol{\theta}) \triangleq & -\boldsymbol{\theta}^T\mathbf{E}_r\bar{\mathbf{Q}}\mathbf{E}_r^T\boldsymbol{\theta} - 2\bar{\mathbf{q}}^T\mathbf{E}_r^T\boldsymbol{\theta} + \frac{\rho}{2}\sum_{l,k}|\tilde{z}_{l,k} - \tilde{r}_{u_k}|^2 \\ & + \frac{\rho}{2}\sum_{l,k}|\hat{z}_{l,k} - \hat{r}_{u_k}|^2 + \frac{\rho}{2}\sum_{l,i}|\tilde{x}_{l,k} - \tilde{r}_{e_k}|^2 + \frac{\rho}{2}\sum_{l,k}|\hat{x}_{l,k} - \hat{r}_{e_k}|^2 \\ & + \frac{\rho}{2}\left(||\mathbf{E}_t^T\boldsymbol{\theta} - \hat{\boldsymbol{\theta}}_t||_2^2\right) + \frac{\rho}{2}\left(||\mathbf{E}_r^T\boldsymbol{\theta} - \hat{\boldsymbol{\theta}}_r||_2^2\right), \end{aligned} \quad (26)$$

where $\tilde{r}_{u_k}$, $\hat{r}_{u_k}$, $\tilde{r}_{e_k}$, $\hat{r}_{e_k}$, $\hat{\boldsymbol{\theta}}_t$, and $\hat{\boldsymbol{\theta}}_r$ are the solutions obtained by projecting $\tilde{z}_{l,i}$, $\hat{z}_{l,i}$, $\tilde{x}_{l,k}$, $\hat{x}_{l,k}$, $\mathbf{E}_t^T\boldsymbol{\theta}$, and $\mathbf{E}_r^T\boldsymbol{\theta}$ onto the feasible sets of (18b)-(18d). Although $G(\boldsymbol{\theta})$ is still nonconvex, by exploiting the strong duality of nonconvex quadratic problem [18], its optimal solution can be obtained as

$$\boldsymbol{\theta} = \mathbf{M}^{-1}\mathbf{N}, \quad (27)$$

where $\mathbf{M} \triangleq -2\bar{\mathbf{Q}}\mathbf{E}_r^T + \rho\mathbf{E}_t\mathbf{E}_t^T + \rho\mathbf{E}_r\mathbf{E}_r^T + \rho\sum_{l,k}\mathbf{E}_t\tilde{\mathbf{v}}_{l,k}^T\tilde{\mathbf{v}}_{l,k}\mathbf{E}_t^T + \rho\sum_{l,k}\mathbf{E}_t\hat{\mathbf{v}}_{l,k}^T\hat{\mathbf{v}}_{l,k}\mathbf{E}_t^T + \rho\sum_{l,k}\mathbf{E}_r\tilde{\mathbf{p}}_{l,k}^T\tilde{\mathbf{p}}_{l,k}\mathbf{E}_r^T + \rho\sum_{l,k}\mathbf{E}_r\hat{\mathbf{p}}_{l,k}^T\hat{\mathbf{p}}_{l,k}\mathbf{E}_r^T + 2\lambda\mathbf{I}_{4N}$, and $\mathbf{N} \triangleq 2\mathbf{E}_r\bar{\mathbf{q}} + \rho\sum_{l,k}\mathbf{E}_t\tilde{\mathbf{v}}_{l,k}^T\tilde{r}_{u_k} + \rho\sum_{l,k}\mathbf{E}_t\hat{\mathbf{v}}_{l,k}^T\hat{r}_{u_k}\rho\sum_{l,k}\mathbf{E}_r\tilde{\mathbf{p}}_{l,k}^T\tilde{r}_{e,l,k} + \rho\sum_{l,k}\mathbf{E}_r\hat{\mathbf{p}}_{l,k}^T\hat{r}_{e,l,k} + \rho\mathbf{E}_r\hat{\boldsymbol{\theta}}_r + \rho\mathbf{E}_t\hat{\boldsymbol{\theta}}_t$.

Algorithm 2 summarizes the proposed distance-majorization induced iterative algorithm for optimizing the transmit and reflective beamforming matrices.

Finally, Algorithm 3 summarizes the proposed iterative algorithm for handling the joint design of $\mathbf{S}$, $\boldsymbol{\Theta}_t$, and $\boldsymbol{\Theta}_r$.

Algorithm 2 Proposed Iterative Algorithm for Problem (18)

1: Initialize $\rho = 1$, $c = 2$, $T = 30$, $\rho_{\max} \gg 1$, $\boldsymbol{\theta}(1) = \boldsymbol{\theta}(0) \in \mathbb{R}^{4N\times 1}$, the convergence tolerance $\epsilon \ll 1$, and $k = 1$.
2: **Repeat**
3: $\mathbf{y}(k) = \boldsymbol{\theta}(k) + \frac{k-1}{k+2}(\boldsymbol{\theta}(k) - \boldsymbol{\theta}(k-1))$,
4: Project $\mathbf{y}(k)$ on the sets defined by (18b)-(18d), and obtain $\hat{\boldsymbol{\theta}}_t$, $\hat{\boldsymbol{\theta}}_r$, $\tilde{\gamma}_{u_k}$, $\hat{\gamma}_{u_k}$, $\tilde{r}_{e_k}$, and $\hat{r}_{e_k}$, $k \in \mathcal{K}_u$, $k \in \mathcal{K}_e$, $l \in \mathcal{L}$.
5: Obtain $\boldsymbol{\theta}$ with (27),
6: Update $\rho = \min(\rho_{\max}, c\rho)$, every T iterations
7: $k = k + 1$,
8: **Until** $||\boldsymbol{\theta}(k+1) - \boldsymbol{\theta}(k)||_2 \leq \epsilon$.

Algorithm 3 Proposed AO Algorithm for the Joint Optimization of $\mathbf{S}$, $\boldsymbol{\Theta}_t$, and $\boldsymbol{\Theta}_r$

1: Initialize the convergence tolerance $\check{\epsilon} = 10^{-1}$,
2: **Repeat**
3: Optimize $\mathbf{S}$ with Algorithm 1,
4: Optimize $\boldsymbol{\Theta}_t$ and $\boldsymbol{\Theta}_r$ with Algorithm 2,
5: **Until** the increase of the objective function is smaller than $\check{\epsilon}$.

IV. Simulation Results

In this section, we adopt Monte Carlo simulations to evaluate the performance of our proposed iterative algorithm. The locations of the BS and the STAR-RIS are $(0\text{ m}, 0\text{ m})$ and $(50\text{ m}, 50\text{ m})$, respectively. The number of users and targets are $K_u = 2$ and $K_e = 3$ respectively, whose locations are generated uniformly in the region of $[0, 100\text{ m}] \times [0, 100\text{ m}]$. In particular, the random locations of the users are $(88.1120\text{ m}, 39.2204\text{ m})$ and $(92.1621\text{ m}, 27.6774\text{ m})$. The locations of the malicious targets are $(28.6037\text{ m}, 73.1042\text{ m})$, $(16.3334m, 73.6524m)$ and $(54.4971\text{ m}, 81.2934\text{ m})$, respectively. Similar to [20], we model the path loss as $35.3 + 37.6\log_{10}l_{\text{ab}}$ (dB), where l_{ab} is the transmission distance from a to b. Unless specified otherwise, the noise power σ^2 is -100 dBm/Hz, the PAPR $\eta = 2.2$, and the Rician factor is 5 dB. Besides, we adopt the orthogonal linear frequency modulation (LFM) as the reference waveform. Then, we set the reference waveform in problem (10) as $\mathbf{s}_0 = \text{vec}(\mathbf{S}_0)$. To validate the efficiency of our proposed distance-majorization induced low-complexity algorithm (DMLCA) in Algorithm 3, following [15], we employ the alternating direction method of multipliers (ADMM) algorithm to introduce the benchmark algorithm.

Fig. 2 shows the convergence rate of our proposed DMLCA, which includes the average radar sensing power achieved by optimizing $\mathbf{S}$ and $(\boldsymbol{\Theta}_r, \boldsymbol{\Theta}_t)$ alternatingly. Clearly, the convergence rate of the proposed DMLCA is fast, which validates its efficiency. Besides, DMLCA has a similar convergence performance for different values of N, which validates its practicability and shows that it enjoys an excellent scalability.

Fig. 3 shows the performance comparison between DMLCA and the ADMM-based algorithm. We set $L = 1$ for facilitating the performance comparison. Clearly, DMLCA achieves better performance than ADMM. Therefore, we can conclude that our proposed DMLCA not only enjoys a much lower complexity than that of ADMM, but also achieves better performance than the latter. Furthermore, to illustrate the benefit introduced

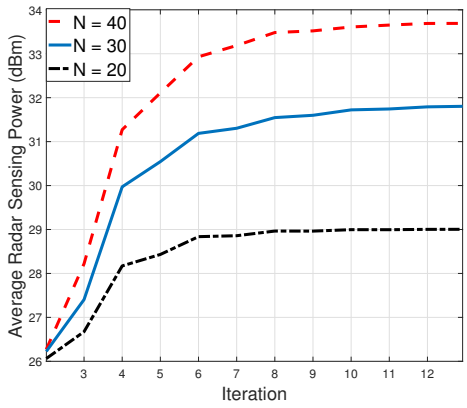

Fig. 2. Convergence of our proposed DMLCA with $N_t = 12$, $K_u = 2$, $K_e = 3$, $P_t = 40$ dBm, $L = 20$, $\epsilon = 0.2$, and different N.

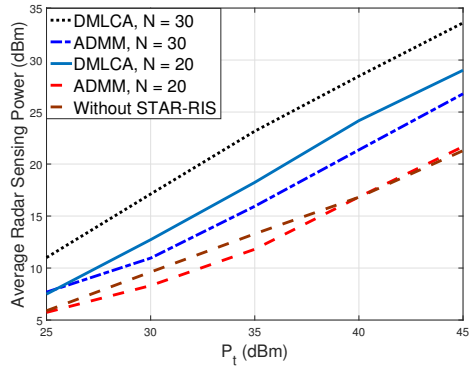

Fig. 3. Performance comparison between our DMLCA and ADMM-based algorithm for different N with $N_t = 12$, $K_u = 2$, $K_e = 3$, $\epsilon = 0.8$, and $L = 1$.

by the STAR-RIS, we also show the DFRC performance in the absence of STAR-RIS denoted as "Without STAR-RIS", whose transmit signal $\mathbf{s}$ is optimized using Algorithm 1. From Fig. 3, we can find that the performance gain brought by STAR-RIS increases with increasing P_t.

V. Conclusion

We proposed a novel symbol-level precoding technique for securing the STAR-RIS-aided DFRC system. Specifically, the multi-user interference is designed to be constructive to legitimate users but is deceptive to Eves by restricting the signals to fall into the constructive region of the public signals. Then, the joint design was formulated as an optimization problem to maximize the radar sensing power subject to the constructive interference constraints for multiple communication users and security constraints for malicious radar targets, as well as the amplitude constraints on the transmission and reflection elements of the STAR-RIS, the PAPR constraint, and the similarity constraint between the transmitted and the reference signals. Although the considered problem is nonconvex, we proposed a distance-majorization induced iterative algorithm to transform the joint design problem into a sequence of subproblems, whose optimal solution in each iteration can be derived in closed-form. Simulation results confirmed the superior performance of our proposed iterative algorithm.

References

[1] F. Liu, Y. Cui, C. Masouros, J. Xu, T. X. Han, Y. C. Eldar, and S. Buzzi, "Integrated sensing and communications: Toward dual-functional wireless networks for 6G and beyond," *IEEE J. Sel. Areas Commun.*, vol. 40, no. 6, pp. 1728–1767, Jun. 2022.

[2] R. Liu, M. Li, Q. Liu, and A. L. Swindlehurst, "Dual-functional radar-communication waveform design: A symbol-level precoding approach," *IEEE J. Sel. Top. Signal Proces.*, vol. 15, no. 6, pp. 1316–1331, Nov. 2021.

[3] X. Liu, T. Huang, N. Shlezinger, Y. Liu, J. Zhou, and Y. C. Eldar, "Joint transmit beamforming for multiuser MIMO communications and MIMO radar," *IEEE Trans. Signal Process.*, vol. 68, pp. 3929–3944, Jun. 2020.

[4] Y. Liu, X. Mu, J. Xu, R. Schober, Y. Hao, H. V. Poor, and L. Hanzo, "STAR: Simultaneous transmission and reflection for 360° coverage by intelligent surfaces," *IEEE Wireless Commun.*, vol. 28, no. 6, pp. 102–109, Dec. 2021.

[5] J. Xu, Y. Liu, X. Mu, R. Schober, and H. V. Poor, "STAR-RISs: A correlated T & R phase-shift model and practical phase-shift configuration strategies," *IEEE J. Sel. Top. Signal Process.*, vol. 16, no. 5, pp. 1097–1111, Sept. 2022.

[6] X. Mu, Y. Liu, L. Guo, J. Lin, and R. Schober, "Simultaneously transmitting and reflecting (STAR) RIS aided wireless communications," *IEEE Trans. Wireless Commun.*, vol. 21, no. 5, pp. 3083–3098, May 2022.

[7] C. Wang, Z. Li, T.-X. Zheng, D. W. K. Ng, and N. Al-Dhahir, "Intelligent reflecting surface-aided full-duplex covert communications: Information freshness optimization," *IEEE Trans. Wireless Commun.*, pp. 1–20, to be published, 2022.

[8] Z. Wang, X. Mu, and Y. Liu, "Stars enabled integrated sensing and communications," *arXiv preprint arXiv:2207.10748*, pp. 1–30, Jul. 2022.

[9] N. Su, F. Liu, and C. Masouros, "Secure radar-communication systems with malicious targets: Integrating radar, communications and jamming functionalities," *IEEE Trans. Wireless Commun.*, vol. 20, no. 1, pp. 83–95, Jan. 2021.

[10] N. Su, F. Liu, Z. Wei, Y.-F. Liu, and C. Masouros, "Secure dual-functional radar-communication transmission: Exploiting interference for resilience against target eavesdropping," *IEEE Trans. Wireless Commun.*, pp. 1–15, Mar. 2022.

[11] C. Wang, Z. Li, J. Shi, and D. W. K. Ng, "Intelligent reflecting surface-assisted multi-antenna covert communications: Joint active and passive beamforming optimization," *IEEE Trans. Commun.*, vol. 69, no. 6, pp. 3984–4000, Jun. 2021.

[12] P. Liu, Y. Li, W. Cheng, X. Gao, and X. Huang, "Intelligent reflecting surface aided NOMA for millimeter-wave Massive MIMO with lens antenna array," *IEEE Trans. Veh. Tech.*, vol. 70, no. 5, pp. 4419–4434, May 2021.

[13] F. Wang, H. Li, and J. Fang, "Joint active and passive beamforming for IRS-assisted radar," *IEEE Signal Process. Lett.*, vol. 29, pp. 349–353, Dec. 2021.

[14] X. Yu, D. Xu, Y. Sun, D. W. K. Ng, and R. Schober, "Robust and secure wireless communications via intelligent reflecting surfaces," *IEEE J. Sel. Areas Commun.*, vol. 38, no. 11, pp. 2637–2652, Nov. 2020.

[15] R. Liu, M. Li, Q. Liu, and A. L. Swindlehurst, "Joint waveform and filter designs for STAP-SLP-based MIMO-DFRC systems," *IEEE J. Sel. Areas Commun.*, vol. 40, no. 6, pp. 1918–1931, Jun. 2022.

[16] P. Stoica, J. Li, and Y. Xie, "On probing signal design for MIMO radar," *IEEE Trans. Signal Process.*, vol. 55, no. 8, pp. 4151–4161, Aug. 2007.

[17] E. C. Chi, H. Zhou, and K. Lange, "Distance majorization and its applications," *Math. Program*, vol. 146, pp. 409–436, Jun. 2014.

[18] S. Boyd and L. Vandenberghe, *Convex Optimization*. Cambridge, U.K.: Cambridge University Press, 2004.

[19] X. Zhang, *Matrix Analysis and Applications*. Second Edition. Beijing, China: Tsinghua University Press, 2013.

[20] C. Wang, Z. Li, H. Zhang, D. W. K. Ng, and N. Al-Dhahir, "Achieving covertness and security in broadcast channels with finite blocklength," *IEEE Trans. Wireless Commun.*, vol. 21, no. 9, pp. 7624–7640, Sept. 2022.